elektrotechnik und
informationstechnik

# Design of hairpin windings considering the transient potential distribution

Jochen Dittmann · Marc England · Bernd Ponick

**Abstract** With the increasing use of novel semiconductor technologies such as SiC and GaN in inverter-fed electrical machines, the switching losses of the power electronics can be reduced. However, this leads to steeper voltage gradients, resulting in a strongly nonlinear transient potential distribution along the winding of the electrical machine. As a result, the insulation system – especially the turn-to-turn insulation – is subjected to additional voltage stress. To carry out targeted dimensioning of the insulation system, it is necessary to calculate the transient potential distribution in advance. In the design of a hairpin winding, it is possible to influence the transient potential differences by employing a method called "shifting" within the winding scheme and thus to reduce the maximum potential differences that occur. On this basis, a targeted design of winding plans with hairpins can be achieved. Here, both the transient potential differences between the conductors within a slot of the stator core and the potential differences between the conductors of different phases in the end winding region of the machine are considered. Furthermore, the voltage differences between the conductors and the stator core are determined and compared for different variants. In this way, it is possible to reduce the amount of material used in the insulation system. Finally, an advantageous winding layout plan based on reduced potential differences is compared with a reference plan.

**Keywords** Hairpin winding · Winding design · End winding · Transient voltage distribution

J. Dittmann (✉) · M. England · B. Ponick
Institute for Drive Systems and Power Electronics, Leibniz University Hannover, Welfengarten 1, 30167 Hannover, Germany
jochen.dittmann@ial.uni-hannover.de

**Entwurf von Haarnadelwicklungen unter Berücksichtigung der transienten Potenzialverteilung**

**Zusammenfassung** Mit dem zunehmenden Einsatz von neuen Halbleitertechnologien wie SiC und GaN bei umrichtergespeisten elektrischen Maschinen können die Schaltverluste der Leistungselektronik reduziert werden. Dies führt jedoch zu größeren Spannungsgradienten, woraus sich eine stark nichtlineare transiente Potenzialverteilung entlang der Wicklung der elektrischen Maschine ergibt. Resultierend wird das Isoliersystem – insbesondere die Windungsisolierung – einer zusätzlichen Beanspruchung ausgesetzt. Um eine gezielte Dimensionierung des Isoliersystems vornehmen zu können, ist es demnach erforderlich, die transiente Potenzialverteilung vorauszuberechnen. Im Entwurfsprozess einer Haarnadelwicklung ist es möglich, durch so genanntes „Shifting" innerhalb des Wicklungsplans die transienten Potenzialdifferenzen zu beeinflussen und somit die maximal auftretenden Potenzialdifferenzen zu reduzieren. Auf dieser Basis kann ein gezieltes Design von Wicklungsplänen mit Hairpins erfolgen. Hierbei werden sowohl die transienten Potenzialdifferenzen zwischen den Leitern innerhalb einer Nut als auch zwischen den Leitern verschiedener Stränge im Endbereich der Maschine berücksichtigt. Außerdem wird das Potenzial zwischen den Leitern und dem Blechpaket identifiziert und für verschiedene Varianten verglichen. Auf diese Weise ist es möglich, den Materialeinsatz für das Isoliersystem zu reduzieren. In einem abschließenden Vergleich wird ein vorteilhafter Nutbelegungsplan auf Basis reduzierter Potenzialdifferenzen einem Referenzplan gegenübergestellt.

**Schlüsselwörter** Haarnadel-Wicklung ·
Wicklungsdesign · Wicklungskopf · Transiente
Spannungsverteilung

## 1 Introduction

The transformation from vehicles propelled by traditional internal combustion engines to battery electric vehicles requires a high degree of automation among all the required components. This requirement also applies to the manufacturing of the electrical machine. Therefore, in more and more applications, rectangular shaped conductors (hairpins) are being used for the stator winding. The degree of automation and the copper filling factor of this winding type are higher than with conventional random round wire windings [1]. In the domain of frequency converters, wide band gap semiconductors such as silicon carbide (SiC) and gallium nitride (GaN) are increasingly being used. In comparison to conventional silicon (Si) semiconductors, these can reduce switching losses through higher switching frequencies and higher voltage gradients [2–4]. However, this also expands the output voltage noise spectra of the inverter and leads to frequencies reaching $f = 100\,\mathrm{MHz}$ [2, 4]. The higher frequency (HF) components cause undesirable side effects in the electrical machine such as bearing currents and higher local voltage stresses.

The focus of this publication is the local voltage stress within the winding of the electrical machine. In order to predict these effects, it is necessary to create a corresponding high-frequency model of the electrical machine. The use of a hairpin winding enables better modelling of HF effects due to the fact that the positions of the conductors within the winding and within the end winding area of the machine are defined, which simplifies the calculation of the HF parameters. The exact conductor position is only subject to the respective production tolerances. In [5–9], different methods for calculating the HF parameters and for creating a machine model based on these parameters are presented. However, these publications explain only how the transient voltage distributions within a given winding can be calculated. The aim of this paper is to show how the voltage distribution can be considered at the time of the design of the winding in order to minimize the local voltage stress.

Fig. 1 shows an overview of the methodological approach to the winding design which considers the voltage distribution. Using the method presented in [10], it is possible to generate hairpin winding plans with good symmetry properties. Based on this method, a reference winding design is created. The positions of the conductors in the winding plan are modified with a novel shifting method. Using the presented filter criteria, the solution space for the shifting method is limited and this results in a manageable number of winding plans. For each of these plans, a calculation of the potential differences is carried
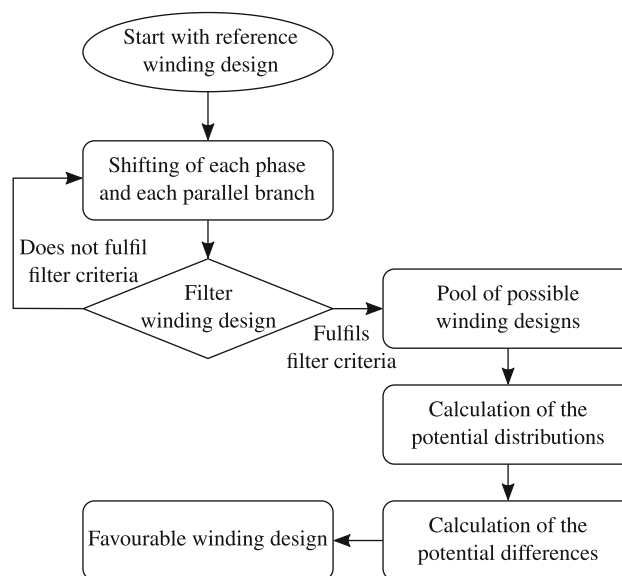


**Fig. 1** Calculation approach to the winding design based on the potential distribution

out. Lastly, a comparison of the maximum potential differences is performed to determine which winding plan has the lowest potential differences.

## 2 Design Guidelines and Reference Machine

For hairpin windings, the rectangular conductors in each slot are arranged in layers. To form a winding, connections between the conductors are made, which are defined by the winding algorithm. General design guidelines for hairpin winding with a multitude of parallel branches per phase are described in [10]. To ensure that no circulating currents are excited, the electrical impedances of all the parallel branches must be equal and the electromotive forces (EMFs) must also be the same. Therefore, two classifications can be derived for hairpin windings affected by saturation effects [11]:

**Table 1** Parameters of the investigated stator sample

| Parameter | Symbol | Value |
|---|---|---|
| No. of pole pairs | $p$ | 3 |
| Statorcore length | $l_{\mathrm{Fe}}$ | 197 mm |
| Stator outer diameter | $D_{\mathrm{o1}}$ | 220 mm |
| Stator inner diameter | $D_{\mathrm{i1}}$ | 140 mm |
| No. of slots | $N$ | 54 |
| No. of layers | $n_{\mathrm{L}}$ | 8 |
| No. of slots per pole and phase | $q$ | 3 |
| Relative permeability of magnetic sheet | $\mu_{\mathrm{r}}$ | 1000 |
| Electric conductivity of magnetic sheet | $\kappa$ | $1.68\,\mathrm{MSm}^{-1}$ |

| Layer / Slot | 1 | 2 | 3 | 4 | 5 | 6 | 7 | 8 | 9 | 10 | 11 | 12 | 13 | 14 | 15 |
|---|---|---|---|---|---|---|---|---|---|---|---|---|---|---|---|
| 1 | 1101 | 1201 | 1301 | 3148 | 3248 | 3348 | 2101 | 2201 | 2301 | 1346 | 1146 | 1246 | 3101 | 3201 | 3301 |
| 2 | 1147 | 1247 | 1347 | 3206 | 3306 | 3306 | 2147 | 2247 | 2347 | 1102 | 1202 | 1302 | 3147 | 3247 | 3347 |
| 3 | 1107 | 1207 | 1307 | 3142 | 3242 | 3342 | 2107 | 2207 | 2307 | 1340 | 1140 | 1240 | 3107 | 3207 | 3307 |
| 4 | 1241 | 1241 | 1341 | 3212 | 3312 | 3112 | 2141 | 2241 | 23 41 | 1108 | 1208 | 1308 | 3141 | 3241 | 3341 |
| 5 | 1113 | 1213 | 1313 | 3136 | 3236 | 3336 | 2113 | 2213 | 2313 | 1334 | 1134 | 1234 | 3113 | 3213 | 3313 |
| 6 | 1135 | 1235 | 1335 | 3218 | 3318 | 3118 | 2134 | 2235 | 2335 | 1114 | 1214 | 1314 | 3135 | 3235 | 3335 |
| 7 | 1119 | 1219 | 1319 | 3130 | 3230 | 3330 | 2119 | 2219 | 2319 | 1328 | 1128 | 1228 | 3119 | 3219 | 3319 |
| 8 | 1129 | 1229 | 1329 | 3224 | 3334 | 3124 | 2129 | 2229 | 2329 | 1120 | 1220 | 1320 | 3129 | 3229 | 3329 |

**Fig. 2** Excerpt from hairpin winding design WD1a3 with $w_1 = 24$ and $a = 3$

| Layer / Slot | 1 | 2 | 3 | 4 | 5 | 6 | 7 | 8 | 9 | 10 | 11 | 12 | 13 | 14 | 15 |
|---|---|---|---|---|---|---|---|---|---|---|---|---|---|---|---|
| 1 | 1171 | 1271 | 1165 | 3172 | 3206 | 3272 | 2171 | 2271 | 2165 | 1202 | 1102 | 1208 | 3171 | 3271 | 3165 |
| 2 | 1201 | 1101 | 1207 | 3160 | 3266 | 3166 | 2201 | 2101 | 2207 | 1164 | 1270 | 1170 | 3101 | 3101 | 3107 |
| 3 | 1159 | 1265 | 1153 | 3106 | 3212 | 3218 | 2159 | 2265 | 2153 | 1214 | 1108 | 1220 | 3159 | 3265 | 3153 |
| 4 | 1213 | 1107 | 1219 | 3148 | 3260 | 3154 | 2213 | 2107 | 2219 | 1152 | 1264 | 1158 | 3213 | 3107 | 3219 |
| 5 | 1147 | 1259 | 1141 | 3112 | 3224 | 3230 | 2147 | 2259 | 2141 | 1226 | 1114 | 1232 | 3147 | 3259 | 3141 |
| 6 | 1225 | 1113 | 1231 | 3136 | 3254 | 3142 | 2225 | 2113 | 2231 | 1140 | 1258 | 1146 | 3225 | 3113 | 3231 |
| 7 | 1135 | 1253 | 1129 | 3118 | 3236 | 3242 | 2135 | 2253 | 2129 | 1238 | 1120 | 1244 | 3135 | 3253 | 3129 |
| 8 | 1237 | 1119 | 1243 | 3124 | 3248 | 3130 | 2237 | 2119 | 2243 | 1128 | 1252 | 1134 | 3237 | 3119 | 3243 |

**Fig. 3** Excerpt from hairpin winding design WD2a2 with $w_1 = 36$ and $a = 2$

1. Weak symmetry: All parallel branches of each phase occupy all layers and independently all phase slots using the same number of conductors;
2. Strong symmetry: All parallel branches of each phase occupy all phase slots in each layer using the same number of conductors.

Weak symmetric designs can lead to circulating currents between parallel branches, resulting in uneven heat distribution due to differing ohmic losses in the parallel branches [11, 12]. This effect is more pronounced for short-pitch windings and in presence of high saturation. For strong symmetric designs, the symmetry is enhanced and no circulating currents are excited.

The design rules for strong symmetry are integrated into a hairpin winding design tool, which considers all possible hairpin designs for given parameters [10]. Considering the parameters in Table 1, winding designs are generated by the tool. Subsequently, favourable designs are chosen on the basis of quality factors. For this research, two different designs are examined. An excerpt from the winding diagram of WD1a3 with an effective number of turns per phase $w_1 = 24$ is shown in Fig. 2. Therein, eight layers and 15 of 54 slots are depicted. The first number represents the phase (1 for phase U). The second number indicates the parallel branch, while the last two numbers describe the interconnection according to the sequential conductor number. As the first conductor is connected to the supply, the last conductor is connected to the star point. Additionally, the phases are distinguished by color and the parallel branches are distinguished by different color intensities. As can be seen from the winding diagram, the winding starts and ends in layer one.

Additionally, a winding design WD3a2 with two parallel branches, as shown in Fig. 3, is chosen. Due to its characteristic that $q \neq a$, a different winding algorithm must be used. Here the winding starts for all phases in layer two and ends in layer one.

Based on these winding designs, the potential differences between conductors are determined and an optimization considering the transient voltage distribution is carried out.

## 3 High Frequency Behaviour of Electrical Machines

During supply of the electrical machine from an inverter, a machine must withstand a sharp pulse-shaped voltage. The switching frequency of the inverter as well as the frequency components show high voltage gradients which lead to additional stress. This may cause bearing currents and EMC interference, for example. Furthermore, these additional frequency components lead to a non-linear voltage drop along the individual turns of a phase. This is due to the geometric arrangement of the individual winding within the electrical machine and the resulting parasitic capacitances and inductances. To predict this behaviour, a fundamental wave model of the electrical machine is no longer sufficient. Instead, it is necessary to model the high frequency behaviour of each individual conductor and then combine this high frequency model into a multi-conductor transmission line model. In Fig. 5, the HF model of two coupled conductors is shown. The conductor model consists of a self-resistance $R_{ii}$ and a self-inductance $L_{ii}$. Furthermore, there is a capacitive coupling to the ground $C_{\mathrm{wf},i}$ and a capacitive coupling to the neighbouring conductors $C_{\mathrm{k},i}$. The dielectric losses of these
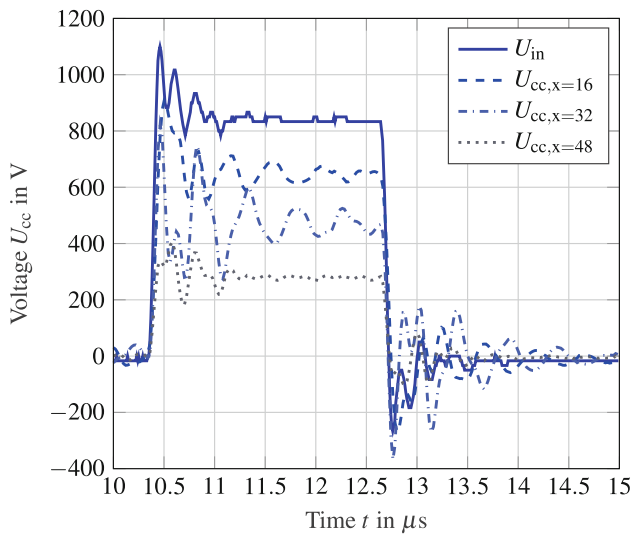
**Fig. 4** Comparison of the measured input voltage $U_{in}$ and different conductor-to-conductor voltages $U_{cc}$ of phase W at the connection variant W-UV over the time

parasitic capacitances are modelled by with $R_{wf,i}$ and $R_{k,i}$. The impedance $Z_{yoke}$ represents the return path through the stator core. The mutual resistance due to an additional voltage drop in conductor $i$ owing a current in conductor $j$ can be represented by $R_{ij}$. Additionally, the inductive coupling between a conductor $i$ and a conductor $j$ is represented by a mutual inductance $L_{ij}$.

Based on the geometric dimensions of the conductors and the stator lamination, the parasitic capacitances between the conductors and to the stator lamination can be determined using FEM or an analytical approach [13]. The fre-quency-dependent resistances and inductances can also calculated using FEM and the parameters of Table 1. The calculation method is well presented in [14] and [15].

With reference to the winding plan as presented in Fig. 2, it is possible to set up the multi-conductor transmission line model as explained in [16], which results in the linear equation system

$$\underbrace{\begin{bmatrix} \mathbf{Y} & \mathbf{B} \\ \mathbf{C} & \mathbf{Z} \end{bmatrix}}_{\mathbf{A}} \underbrace{\begin{bmatrix} \mathbf{U} \\ \mathbf{I} \end{bmatrix}}_{\mathbf{x}} = \underbrace{\begin{bmatrix} \mathbf{I}_q \\ \mathbf{U}_q \end{bmatrix}}_{\mathbf{b}}. \qquad (1)$$

$\mathbf{Y}$ is the admittance matrix and $\mathbf{B}$ contains the nodal equations in combination with x and b. The matrix $\mathbf{C}$ represents additional relationships of the network branches and the impedance matrix $\mathbf{Z}$ contains the self-inductances and the mutual inductances. The equation system can be solved by using the modified nodal analysis

$$\mathbf{x} = \mathbf{A}^{-1}\mathbf{b} \qquad (2)$$
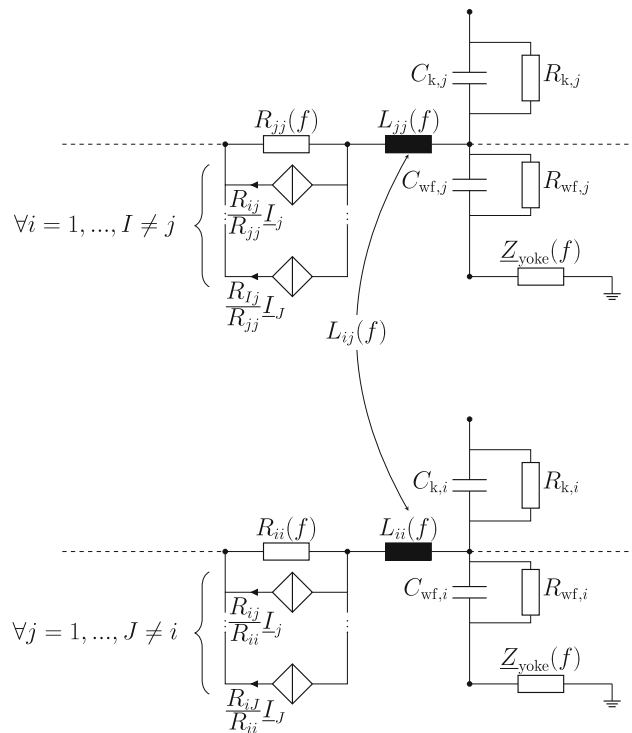


**Fig. 5** High frequency model of coupled conductors [18]

in the frequency domain. As a result of the nodal analysis, according to [17], $\mathbf{U}$ contains the complex node potentials. With

$$\underline{H}(x,f) = \frac{\underline{U}(x,f)}{\underline{U}_{q1}(f)}, \qquad (3)$$

it is possible to determine the transfer function of every node in the model, which describes the relationship between the input voltage signal and the respective node voltage. Additionally, [17] presents an approach used to calculate the potential distribution caused by a given input voltage pulse. The method involves a simple multiplication of the input voltage and the transfer function of each node voltage in the frequency domain. By using the inverse Fourier transform it is possible to obtain the space- and time-dependent voltage signal of each node in the multi-conductor transmission line model. In Fig. 6, the geometric positions of the calculated potentials are shown. It can be seen that the potential is always calculated at a point after the conductor has passed through the stator core. In the end winding region (welding side and bending side), it is assumed that the potential is constant.

## 4 Potential Differences of Hairpin Windings

### 4.1 General

By using an inverter-fed electrical machine, different connections of the stator winding occur due to
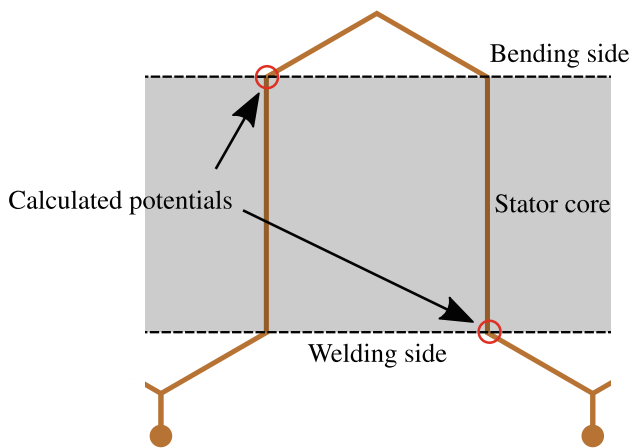
Fig. 6    Geometric positions of the calculated potentials



Fig. 7    Comparison of the spatial potential distributions of different DM connections at the same point in time

the switching behaviour of the semiconductors. Besides the common-mode connection, these also include the three different differential-mode (DM) connections. Due to the fact that perfect symmetry between the different phases is not possible, the three connection variants U-VW, V-UW and W-UV have to be investigated separately. Fig. 7 shows the asymmetric behaviour of the three different DM connections at the same point in time. This asymmetry does not refer to the method presented in [11] which is used to reduce circulating currents within the winding. Each position within the slots in the machine has different parasitic HF characteristics. This is due to the capacitive and inductive couplings of the stator core and to the immediately surrounding conductors. A perfectly symmetrical potential distribution would therefore require that the same couplings always occur for the different phases and parallel branches in the spatial distribution. However, this cannot be realised within a coherent winding. The asymmetrical behaviour shown here has no influence on the fundamental operational behaviour of the electrical machine.

The differences shown in Fig. 7 result from the spatially different distribution of the conductors along the winding within the stator core. In this winding plan, the different step widths of the individual parallel branches on the bending side lead to an asymmetrical potential distribution between the three phases. Even a short-pitched winding can lead to stronger asymmetrical behaviour and thereby to greater differences between the potential distributions of the individual phases and parallel branches. Therefore, it is necessary to simulate all four connection variants when investigating the maximum potential differences which can occur in a winding plan.

### 4.2  Stator Core

Based on the existing winding diagram shown in Fig. 2 and Fig. 3, it is possible to determine the potential differences within a slot after calculating the four dif-
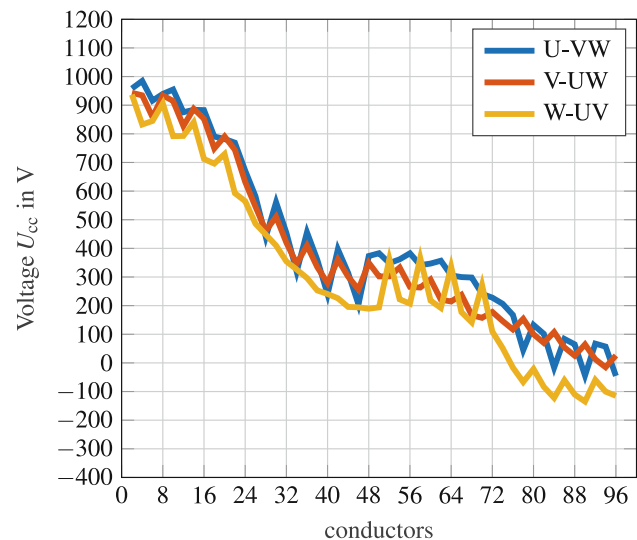
ferent connection variants. For this purpose, the potential differences of directly adjacent conductors are calculated and the potential of all conductors relative to the laminated core is determined.

### 4.3  End Winding Region

For the calculation of the potential differences within the two end winding regions of the electrical machine, it is necessary to identify all spots where the conductors of two different layers cross each other. Fig. 8 shows a simplified bending side of the winding with only two layers and six conductors. It can be seen that the conductor C1 crosses the conductors C4, C5 and C6 by passing the end winding region until it reaches the bending point. At this point, the conductor is not only bent to re-enter the stator core, but a change of layer also takes place, so that a conductor that exits the stator core from layer two re-enters the stator core in the layer above or below layer two. This results in conductor C1 crossing conductors C2 and C4 between the bending point and its re-entry into the stator core.

By expanding the simple example shown in Fig. 8 to add more layers per slot, additional conductors are introduced above and below the conductors C1, C2 and C3. Even these conductors change layer in the end winding region, which leads to further crossings and thus to new potential differences. Based on these conductor paths, a pattern can be prepared which identifies the conductors for which crossings occur within the end winding region. Fig. 9 shows this pattern for the conductor 1213. The conductor exits the stator core from slot 1, layer 4 and reenters the stator core in slot 10, layer 3. These positions are marked in blue. The layer change of a conductor always takes place at the geometric centre between the entry and exit points in the stator core. In this example, it is between slot 5 and slot 6. The cells marked in yellow contain
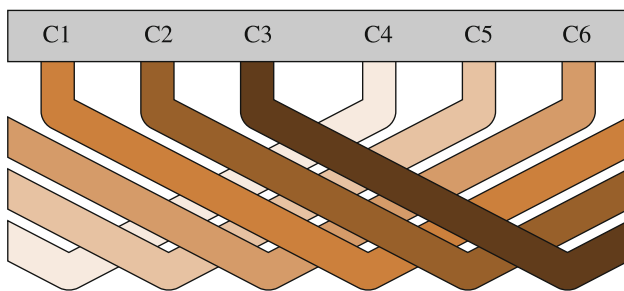
**Fig. 8** Excerpt from a hairpin end winding region

| Layer / Slot | 1 | 2 | 3 | ... | 8 | 9 | 10 |
|---|---|---|---|---|---|---|---|
| 1 | 1171 | 1271 | 1165 | ... | 2271 | 2165 | 1202 |
| 2 | 1201 | 1101 | 1207 | ... | 2101 | 2207 | 1164 |
| 3 | 1159 | 1265 | 1153 | ... | 2265 | 2153 | 1214 |
| 4 | 1213 | 1107 | 1219 | ... | 2107 | 2219 | 1152 |
| 5 | 1147 | 1259 | 1141 | ... | 2259 | 2141 | 1226 |
| 6 | 1225 | 1113 | 1231 | ... | 2113 | 2231 | 1140 |
| 7 | 1135 | 1253 | 1129 | ... | 2253 | 2129 | 1238 |
| 8 | 1237 | 1119 | 1243 | ... | 2119 | 2243 | 1128 |

**Fig. 9** Resulting pattern for the calculation of the potential differences on the bending and on the welding sides of the end winding region

the conductors crossed by conductor 1213 and therefore all potential differences which need to be calculated. This pattern can now be used to determine all potential differences within the end winding region. For the top and bottom layers, an adapted pattern is defined.

## 5 Shifting

To influence the potential differences without changing the winding layout itself, a shifting method is employed. To explain conductor shifting, an excerpt from an unshifted reference winding of phase U is shown in Fig. 10. The parallel branches $a_1$ and $a_2$ start in slot 1 and slot 2 of layer 1, respectively. The winding pattern connects the individual conductors of each winding zone as shown. If a shift is applied, the conductor positions remain the same, but the numbering changes. For example, a shift by one position $n_{shift} = 1$ means that the conductor connected to the supply line is moved by two winding zones, so that the winding for parallel path $a_1$ starts in slot 13. This is shown for an even shift for $a_1$ and $a_2$ in Fig. 11. If a shift by two positions $n_{shift} = 2$ is executed, the winding shown in Fig. 12 results.

The shifting method can be performed equally for all parallel branches as depicted here, or individually for each parallel branch. Also, each phase can be shifted by a different step, so that the start and the end conductors of each phase are located in different slots and layers. Thereby, this method influences the potential differences between the conductors and the potential differences between the conductors and ground. Fig. 13 shows the influence of $n_{shift} = 1$ and $n_{shift} = 2$ shifted winding plans of the WD1a3 winding design on the spatial potential distribution. It can be seen that the spatial potential distribution depends on the spatial conductor distribution in the stator core. By using the shifting method, the spatial conductor distribution changes and therefore the potential distribution is also affected. Furthermore, it can be seen that some local minima occur in the spatial potential distribution. At the locations of the local minima, a special hairpin connects layers 1-2 to layers 3-4. By using the shifting method, the conductor number which gets assigned with this special hairpin

also changes. This leads to a shift of these local minima due to the change in the conductor position, and thereby to changes in both, the capacitive coupling and the inductive coupling, caused by the spatial potential distribution. At conductor 48, the star point is located. Above the star point, the parallel connection of the phases 2 and 3 can be found. Therefore, there is no displacement of the spatial potential distribution above the conductor 48, since only the first phase was shifted. When considering the spatial potential distribution over time, it can be seen that an oscillation occurs between the special hairpins.

Beside the described minima and the oscillation, the spatial potential distribution of the $n_{shift} = 2$ shifted winding plan reaches higher peak values of the potential difference. Moreover, at the conductor 24 of the reference winding plan, there is a nearly linear course of the potential distribution. At this conductor, the last layer in the stator slot is reached. Now, the winding algorithm changes the direction to fill the slots from the last layer to the first layer. Thereby, a change in the spatial potential distribution also occurs. This direction change is performed twice per phase and leads to another oscillation of the potential distribution between these positions over time. In summary, each change in the conductor position within the winding plan leads to a change in the spatial potential distribution. Therefore, the shifting method can be used to optimise the winding plan to achieve a lower voltage stress.

## 6 Filtering Process

By using the shifting method, it is possible to shift each phase and also each parallel branch separately. This leads to large degree of freedom and thereby to a high number of possible winding plans. A calculation of the potential distribution for each winding plan would demand high computational resources. Therefore, it is necessary to filter the list of possible winding plans. For the optimisation of the winding plan, the following filter criteria are introduced, which must be fulfilled by the shifted winding plans.

1. Phase input slot: The input conductor of each parallel branch of each phase must be in the range of
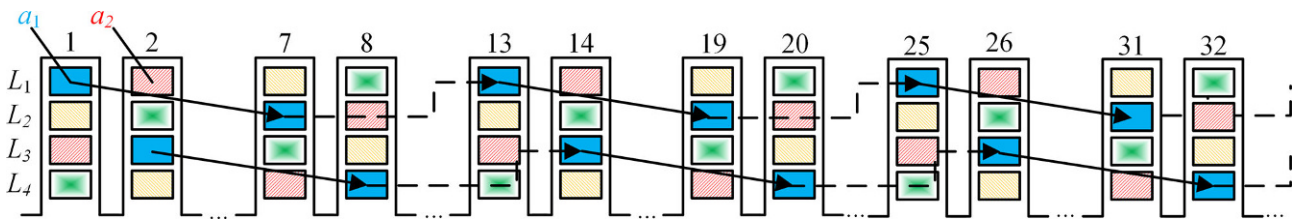
**Fig. 10** Excerpt of phase U of an unshifted winding design with $Q = 48$, $p = 4$, $q = 4$, $n_L = 4$, $a = 4$; different parallel branches are differentiated by color
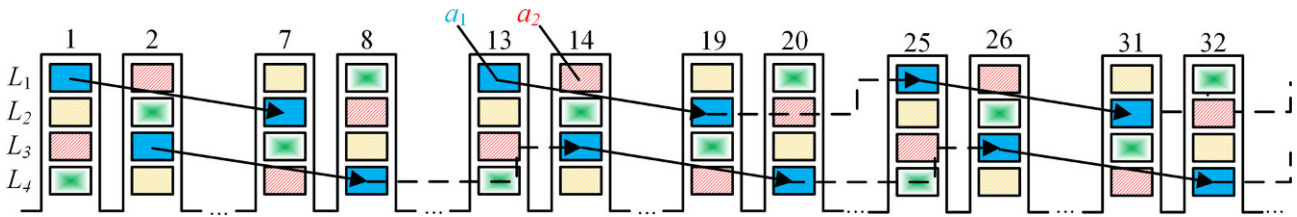


**Fig. 11** Excerpt of phase U of an $n_{shift} = 1$ shifted winding design with $Q = 48$, $p = 4$, $q = 4$, $n_L = 4$, $a = 4$; different parallel branches are differentiated by colour



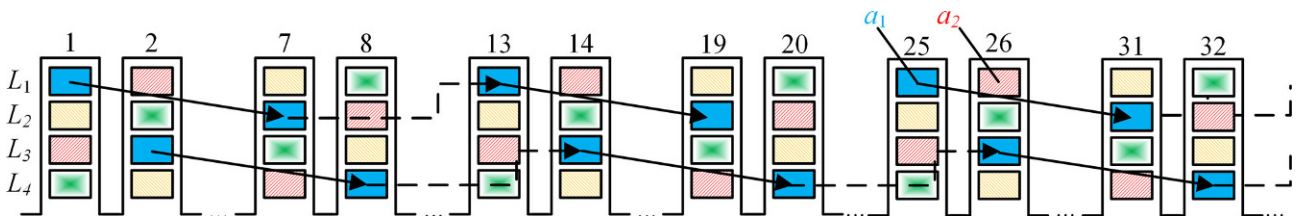**Fig. 12** Excerpt of phase U of an $n_{shift} = 2$ shifted winding design with $Q = 48$, $p = 4$, $q = 4$, $n_L = 4$, $a = 4$; different parallel branches are differentiated by color

$N_{diff} = 2q - 1$ slots. Fig. 14 shows this range with the parameter $N_{diff}$. This criterion is required to ensure the shortest and most symmetrical connection cables to the inverter.

2. Phase output layer: The output conductor of each parallel branch of each phase must be in the range one layer deeper or higher, i.e., ± 1 layer. This filter criterion enables a short and simple star point connection.

By using these two filter criteria, the number of possible winding plans can be reduced. This results in 368 different shifted plans for WD1a3 and 272 different shifted plans for WD2a2. For each of these plans, a calculation of the potential distribution and the potential differences is performed.

## 7 Comparison of Shifted and Unshifted Designs

After the shifting and filtering processes have been completed, calculations of the three DM connections and the CM connection are performed for each winding plan. To compare the different winding plans after this, it is necessary to define a comparable value. This must be composed of the maximum conductor-to-conductor voltage $U_{max,cc}$ and the maximum con-

ductor-to-ground voltage $U_{max,cGND}$ occurring in each winding plan. Therefore, the comparison voltage

$$U_{comp} = \sqrt{U_{max,cGND}^2 + U_{max,cc}^2} \qquad (4)$$

is introduced. It is the geometric sum of the two calculated maximum voltages for each winding plan. Fig. 15 shows the values of voltage $U_{comp}$ for the winding designs WD1a3 and WD2a2. It can be seen that there is a global minimum for the WD1a3 winding design at the winding plan number 122 with $U_{comp} = 1392$ V. Furthermore, a maximum can be identified for the winding plan 161 at $U_{comp} = 1859$ V. This results in a voltage difference between the maximum and the minimum of $U_{shift,diff} = 467$ V. In Table 2, further voltage differences between the unshifted reference winding and the shifted winding are listed. It can be seen that the shifting method can reduce the maximum voltage stress that occurs both between the conductors and between the conductors and the stator core. Furthermore, it can be seen that the maximum voltage between the conductors can always be found in the end winding region. The voltage differences within the stator core are relatively low. This is due to the fact that voltage differences between the different phases are only determined in the end winding region. Within a slot, however, there is always
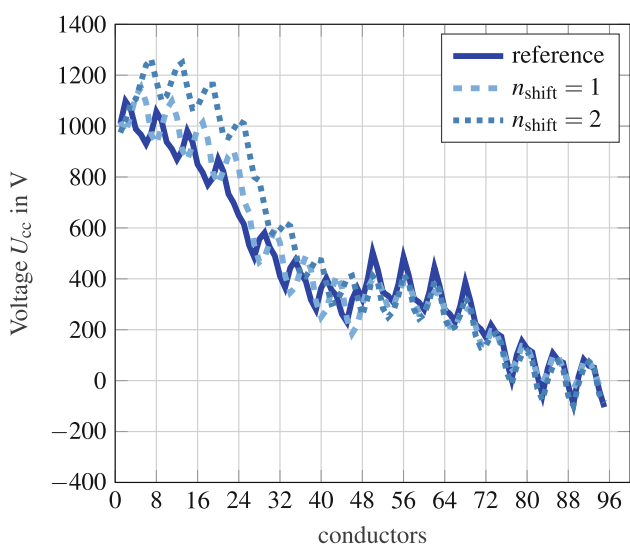
**Fig. 13** Comparison of the spatial potential distributions of the reference $n_{\text{shift}} = 1$ and an $n_{\text{shift}} = 2$ shifted phase 1 of the WD1a3 winding design at the same point in time
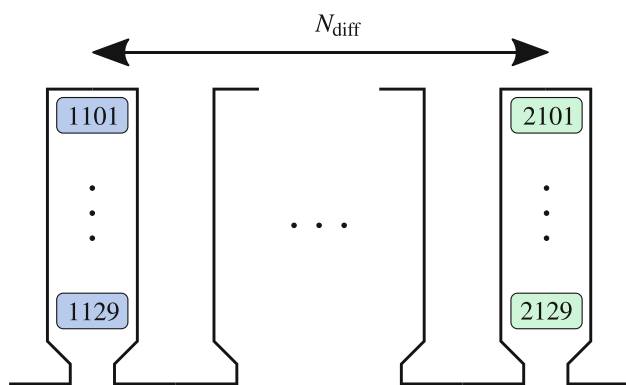


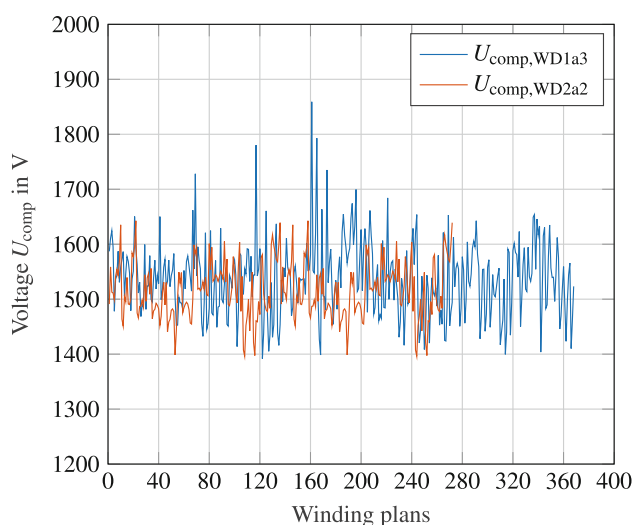**Fig. 14** Visualisation of the filter parameter $N_{\text{diff}}$



**Fig. 15** Values of the comparison voltage $U_{\text{comp}}$ of the WD1a3 and the WD2a2 winding plan at the same point in time
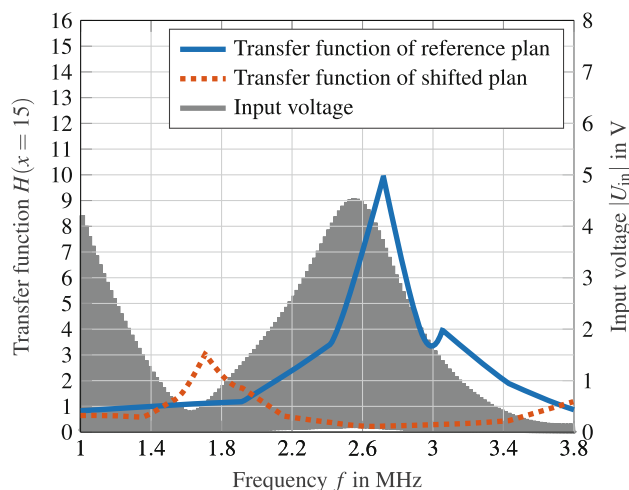


**Fig. 16** Comparison of the transfer function $|H(x=15)|$ from the reference and the shifted winding plans based on the winding design WD1a3 together with a plot of the input voltage spectrum $U_{\text{in}}$

just a single phase, which would only change by using a short-pitch winding and thus a change in the winding design. By optimizing the winding design WD2a2, it is possible to reduce the voltage between adjacent conductors $U_{\text{max,cc}}$ by 7.4 % and the voltage between the conductors and the stator core $U_{\text{max,cGND}}$ by 16,6 %.

For the winding design WD1a3, the conductor-to-conductor voltage $U_{\text{max,cc}}$ can be reduced by 7.7 % and the conductor-to-ground voltage $U_{\text{max,cGND}}$ by 45 % if shifting is employed. In order to analyse the high difference in $U_{\text{max,cGND}}$ between the reference plan and the shifted plan in detail, the two transfer functions $H(x=15)$ of the conductor 15 of phase W and the parallel branch 2 in the frequency domain are shown in Fig. 16. This chosen conductor represents the position where the highest voltage stress occurs. In addition, the spectrum of the input voltage $|U_{\text{in}}|$ is shown, which excites the system. It can be seen that the transfer function of the reference plan has a sharply formed resonance at a frequency of $f = 2.7$ MHz. This reso-

nance is moved to the lower frequency range in the shifted plan and has a reduced amplitude. The spectrum of the input voltage shows large amplitudes in the range between $f = 2$ MHz and $f = 3$ MHz which, in combination with the resonance of the reference plan, leads to the voltage spike in the time domain.

## 8 Conclusion

This paper shows a method for the design of a hairpin winding which considers the transient voltage distribution. Starting from different reference winding designs, it explains how the shifting method can adjust winding plans without changing the underlying design. In order to limit the solution space of the possible winding plans, filter criteria were introduced

**Table 2** Comparison of the maximum voltage differences occurring in the shifted and the unshifted winding designs

| Winding design | $U_{max,cc}$ | $U_{max,cc,slot}$ | $U_{max,cc,ew}$ | $U_{max,cGND}$ |
|---|---|---|---|---|
| WD1a3 reference | 1241 V | 963 V | 1241 V | 1355 V |
| WD1a3 var.122 | 1145 V | 740 V | 1145 V | 731 V |
| WD2a2 reference | 1288 V | 911 V | 1289 V | 849 V |
| WD2a2 var.108 | 1193 V | 828 V | 1193 V | 725 V |

which make an investigation of the transient voltage distribution feasible. Based on the winding diagrams, multi-conductor transmission-line models are created and solved with the help of the modified nodal analysis in the frequency domain. Subsequently, the potential distributions of the different connections were determined by applying a measured input voltage pulse to the system. Moreover, two methods to calculate the voltage differences within the stator core and within the end winding region are presented. A comparison of the maximum voltage differences between the unshifted and the shifted winding plans shows a substantial variation and thus good potential for optimization. Furthermore, the origin of the higher voltages can be explained by the interaction between the transfer functions and the voltage spectrum of the input voltage. Considering the calculated maximum voltages, a design for the insulation system of the electrical machine can be prepared. Nevertheless, it is necessary to consider the interactions between the inverter, the cable and the electrical machine to avoid matches between the excitation voltage and resonant frequencies of the winding, which would lead to high local voltage stresses.

## References

1. J. Juergens, A. Fricassè, L. Marengo, J. Gragger, M. De Gennaro, and B. Ponick, "Innovative design of an air cooled ferrite permanent magnet assisted synchronous reluctance machine for automotive traction application," pp. 803–810, 2016.
2. D. Han, S. Li, Y. Wu, W. Choi, and B. Sarlioglu, "Comparative analysis on conducted cm emi emission of motor drives: Wbg versus si devices," *IEEE Transactions on Industrial Electronics,* vol. 64, no. 10, pp. 8353–8363, 2017.
3. A. Merkert, T. Krone, and A. Mertens, "Characterization and scalable modeling of power semiconductors for optimized design of traction inverters with si- and sic-devices," *IEEE Transactions on Power Electronics,* vol. 29, no. 5, pp. 2238–2245, 2014.
4. N. Oswald, P. Anthony, N. McNeill, and B. H. Stark, "An experimental investigation of the tradeoff between switching losses and emi generation with hard-switched all-si, si-sic, and all-sic device combinations," *IEEE Transactions on Power Electronics,* vol. 29, no. 5, pp. 2393–2407, 2014.
5. M. Keller, M. Maier, T. Petri, and N. Parspour, "Modelling the dynamic voltage distribution in electric traction motor windings," 2022.
6. X. Ju, Y. Cheng, M. Yang, S. Cui, A. Sun, X. Liu, and M. He, "Voltage stress calculation and measurement for hairpin winding of ev traction machines driven by sic mosfet," *IEEE Transactions on Industrial Electronics,* vol. 69, no. 9, pp. 8803–8814, 2022.
7. E. Preci, S. Nuzzo, D. Barater, D. Gerada, M. Degano, G. Buticchi, and C. Gerada, "Modelling of voltage distribution within hairpin windings," pp. 1–6, 2021.
8. M. Pastura, S. Nuzzo, D. Barater, and G. Franceschini, "Analysis of voltage distribution and connections within a high-frequency hairpin winding model," pp. 1642–1647, 2022.
9. G. Berardi, S. Nategh, and N. Bianchi, "Inter-turn voltage in hairpin winding of traction motors fed by high-switching frequency inverters," vol. 1, pp. 909–915, 2020.
10. M. England and B. Ponick, "Automatisierter Entwurf von Haarnadelwicklungen anhand von tabellarischen Belegungsplänen," *e + i Elektrotechnik und Informationstechnik,* vol. 136, pp. 159–67, 03 2019.
11. M. England, B. Dotz, and B. Ponick, "Evaluation of winding symmetry and circulating currents of hairpin windings," pp. 1–8, 2021.
12. G. Venturini, M. Carbonieri, L. Di Leonardo, and M. Popescu, "Hairpin windings for traction machines: Analysis and comparison," pp. 1655–1661, 2022.
13. J. Stockbrügger, A. Hoffmann, B. Knebusch, J. Dittmann, and B. Ponick, "Analytische Ermittlung der Leiter-Leiter-Kapazität von Zweischichtwicklungen unter Berücksichtigung des Zwischenschiebers zur Vorausberechnung der Potenzialverteilung in der Ständerwicklung umrichtergespeister elektrischer Maschinen," *e + i Elektrotechnik und Informationstechnik,* vol. 138, pp. 1–8, 03 2021.
14. H. Kaden, *Wirbelströme und Schirmung in der Nachrichtentechnik.* Berlin, Heidelberg: Springer, 2006.
15. R. L. Stoll, *The analysis of eddy currents, Monographs in electrical and electric engineering.* Oxford: Clarendon Press;, 1974.
16. C.-N. Behrendt, J. Dittmann, B. Knebusch, and B. Ponick, "Common-mode impedance prediction of a high frequency hairpin stator winding based on fem and modified nodal analysis," pp. 20–26, 2022.

**Originalarbeit**

17. J. Dittmann, C.-N. Behrendt, and B. Ponick, "Prediction of the voltage distribution in a inverter-fed hairpin stator winding," to be published at *2022 International Conference on Electrical Machines and Systems (ICEMS)*.
18. C.-N. Behrendt, J. Dittmann, B. Knebusch, and B. Ponick, "An investigation into the trade-off between full machine and single-slot fem simulations for electrical machine modeling at high frequencies with respect to inter-wire couplings," pp. 2242–2248, 2022.

**Publisher's Note** Springer Nature remains neutral with regard to jurisdictional claims in published maps and institutional affiliations.

**Jochen Dittmann,** was born in Ilmenau, Germany, in Juni 1990. He received the Master of Science degree in electrical engineering from the Leibniz University Hannover in 2019. Since 2019 has been working as a research associate at the Institute for Dive Systems and Power Electronics. His research interests include the high frequency effects in electrical machines.
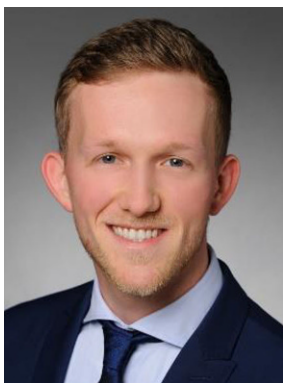
**Marc England,** studied power engineering at Leibniz University Hannover, Germany and received his Master of Science degree in January 2018. Following his studies, he has been employed as a research associate at the Institute of Drive Systems and Power Electronics at Leibniz University Hannover. His research interests are in the area of dimensioning of hairpin windings and reduction of torque ripple as well as investigation of the acoustic behavior of traction machines.

**Bernd Ponick,** was born in Großburgwedel, Germany, in 1964. He received his Dipl.-Ing. degree in electrical power engineering from the University of Hannover in 1990 and his Dr.-Ing. degree for a thesis on electrical machines in 1994. After 9 years with the Large Drives Division of Siemens as design engineer for large variable speed motors, head of electrical design and Technical Director of Siemens Dynamowerk Berlin, he has worked since 2003 as full professor for electrical machines and drive systems at Leibniz University Hannover. His main research activities are calculation and simulation methods for electrical machines, prediction of and measures to mitigate important parasitic effects such as magnetic noise, additional losses or bearing currents, and new applications for electrical machines, e.g., for electric vehicles or aviation.